

Topological metal bands with double-triple-point fermions in optical lattices

Xue-Ying Mai,¹ Yan-Qing Zhu,² Zhi Li,¹ Dan-Wei Zhang,^{1,*} and Shi-Liang Zhu^{2,1,†}

¹*Guangdong Provincial Key Laboratory of Quantum Engineering and Quantum Materials, SPTE, South China Normal University, Guangzhou 510006, China*

²*National Laboratory of Solid State Microstructures and School of Physics, Nanjing University, Nanjing 210093, China*
(Dated: March 14, 2022)

Novel fermionic quasiparticles with integer pseudospins in some energy bands, such as pseudospin-1 triple-point fermions, recently attract increasing interest since they are beyond the conventional spin-1/2 Dirac and Weyl counterparts. In this paper, we propose a class of pseudospin-1 fermionic excitations emerging in topological metal bands, dubbed double-triple-point (DTP) fermions. We first present a general three-band continuum model with C_4 symmetry in three dimensions, which has three types of threefold degenerate points in the bands classified by their topological charges $C = \pm 4, \pm 2, 0$, respectively. They are dubbed DTPs as spin-1 generalization of double-Weyl points. We then construct two-dimensional and three-dimensional tight-binding lattice models of topological metal bands with exotic DTP fermions near the DTPs. In two dimensions, the band gaps close at a trivial DTP with zero Berry phase, which occurs at the transition between the normal and topological insulator phases. In three dimensions, the topological properties of three different DTP fermions in lattice systems are further investigated, and the effects of breaking C_4 symmetry are also studied, which generally leads to splitting each quadratic DTP into two linear triple points and gives topological phase diagrams. Using ultracold fermionic atoms in optical lattices, the proposed models can be realized and the topological properties of the DTP fermions can be detected.

I. INTRODUCTION

Topological semimetals and metals, such as Dirac and Weyl semimetals, have recently attracted broad attentions due to their interesting fundamental physics and potential applications [1]. In three-dimensional (3D) Weyl semimetals, the low-energy excitations near twofold band crossings dubbed as Weyl points resemble the well-known Weyl fermions in particle physics [2–10]. The Weyl fermions have linear dispersion along all three momenta directions [see Fig. 1(a)] governed by the effective Weyl Hamiltonian, and a pair of Weyl points carry topological charges $C = \pm 1$, which support gapless Fermi arc surface states. Both the Weyl fermions (points) in the bulk and Fermi arcs in the surface give rise to exotic phenomena, such as anomalous electromagnetic responses [1]. In another class of Weyl semimetals, the multi-Weyl semimetals [11–13], the twofold band degeneracies carry topological charges of higher magnitudes and can be stabilized by certain point-group crystal symmetries. Particularly, the double-Weyl points in double-Weyl semimetals have topological charges $C = \pm 2$ and linear dispersion only along one dimension but quadratic along the other two dimensions [see Fig. 1(b)], near which the low-energy excitations are called as double-Weyl fermions [11–13].

Very recently, considerable attention have been paid to searching for unconventional massless fermionic excitations beyond Dirac and Weyl paradigm [14–28]. In contrast to particles in high-energy physics constrained by Poincaré symmetry, quasiparticles in a lattice system

are only constrained by certain subgroups (space groups) of the Poincaré symmetry, which allows the emergence of “new fermions” (fermionic quasiparticles beyond the Dirac-Weyl-Majorana classification) in some band structures with three- or morefold degeneracies [14]. In particular, triple-point (three-component) fermions as spin-1 generalization of Weyl fermions in certain topological metal bands with threefold degeneracies were theoretically predicted and then experimental observed in some condensed matter materials [15, 23]. Similar to the spin-1/2 Weyl fermions, the spin-1 triple-point fermions have linear dispersion along all momentum directions near the threefold degenerate points, which carry topological charges $C = \pm 2$ [14, 24] [see Fig. 1(c)]. Along this direction, an important question then is whether other types of triple-point fermions can emerge in topological metal bands, such as the spin-1 generalization of double-Weyl fermions [see Fig. 1(d)] that are yet to be studied.

On the other hand, it has been shown that ultracold atoms in optical lattices with synthetic gauge fields and spin-orbit coupling provide a promising platform for studying topological states and phenomena [29–34]. Remarkably, Dirac fermions in a tunable honeycomb optical lattice [35, 36] has been realized [37], where the topological phase transition and the π Berry phase of a Dirac point have been directly observed [38]. The celebrated Harper-Hofstadter model [39] and Haldane model [40] have been realized with cold atoms in two-dimensional (2D) optical lattices [41–45], where the Chern numbers characterizing the band topology have also been measured. The experimental observation of chiral edge states with cold atoms in synthetic Hall ribbons has been reported [46, 47]. The topological (geometric) pumping [48, 49] has been demonstrated in optical superlattices [50–53]. The 2D spin-orbit coupling and topological

*Electronic address: danweizhang@m.scnu.edu.cn

†Electronic address: slzhu@nju.edu.cn

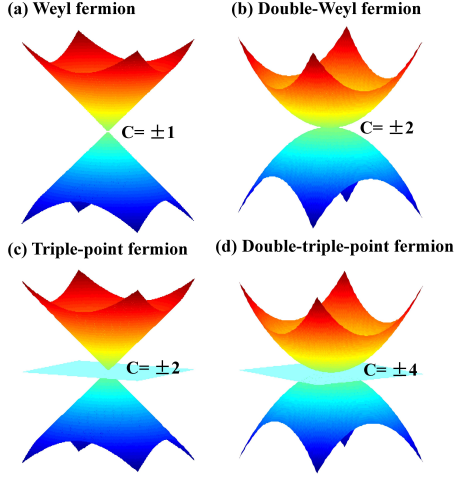


FIG. 1: (Color online) Energy dispersions of (a) Spin-1/2 Weyl fermions; (b) Spin-1/2 double-Weyl fermions; (c) Spin-1 triple-point fermions; (d) Spin-1 double-triple-point fermions. The corresponding topological charges of the band degenerate points are shown.

bands have been generated in an optical Raman lattice [54, 55]. In addition, several schemes have been suggested to realize topological semimetal bands with Weyl fermions [56–66] and double-Weyl fermions [67, 68]. Moreover, it has been proposed that the spin-1 triple-point fermions can emerge in some topological metal bands in cold atom systems [24–26], which can even be simulated in parameter space [69, 70]. Due to the elusive nature of triple-point fermions in real materials and their exotic properties [14–26], proposals for realizing other types of triple-point fermions in artificial cold atom systems would be of great value.

In this paper, we propose a new class of spin-1 fermionic excitations emerging in topological metal bands, which are dubbed double-triple-point (DTP) fermions as the spin-1 generalization of double-Weyl fermions. We first present a general three-band continuum model with C_4 symmetry in 3D, which is shown to contain three different types of threefold degenerate points in the bands classified by their topological charges $C = \pm 4, \pm 2, 0$, respectively. The threefold degenerate points are called as DTPs as spin-1 double-Weyl points. We then construct 2D and 3D tight-binding lattice models of topological metal bands with DTP fermions near the DTPs, respectively. In 2D, the bands close at a trivial DTP with zero Berry phase, which occurs at the transition between the normal and topological insulator phases. In 3D, the topological properties of three different DTP fermions in lattice systems are further investigated, such as the bulk-edge correspondence. The effects of breaking C_4 symmetry in this case are also studied, which generally leads to splitting each DTP into two triple points and gives topological phase diagrams. Finally, we discuss the realization of the models and detection of the topological properties of the DTP fermions with ultracold fermionic

atoms in optical lattices.

The paper is organized as follows. In Sec. II, we construct a continuum model with three types of DTPs. In Section III, we study DTP fermions in a 2D tight-binding lattice model. In Sec. IV, the topological properties of three different DTP fermions in 3D lattice systems are further investigated. In Sec. V, we propose realization of the models and detection of the the DTP fermions in optical lattices. A brief conclusion is finally given in Sec. VI.

II. A CONTINUUM MODEL

Let us begin with a three-band continuum model with a symmetry C_4 in 3D, which takes the following Hamiltonian

$$\mathcal{H}(\mathbf{k}) = (k_y^2 - k_x^2)S_x + k_x k_y S_y + k_z(\alpha S_z + \beta N_{ij}), \quad (1)$$

where α and β are parameters, $\mathbf{S} = (S_x, S_y, S_z)$ are the spin-1 matrices given by [24]

$$S_x = \begin{pmatrix} 0 & 0 & 0 \\ 0 & 0 & -i \\ 0 & i & 0 \end{pmatrix}, S_y = \begin{pmatrix} 0 & 0 & i \\ 0 & 0 & 0 \\ -i & 0 & 0 \end{pmatrix}, S_z = \begin{pmatrix} 0 & -i & 0 \\ i & 0 & 0 \\ 0 & 0 & 0 \end{pmatrix}, \quad (2)$$

and N_{ij} are the tensors given by [26] $N_{ij} = (S_i S_j + S_j S_i)/2 - \delta_{ij} \mathbf{S}^2/3$ ($i, j = x, y, z$). Note that the spin-1 matrices satisfy that $[S_x, S_y] = iS_z$, $\mathbf{S} \times \mathbf{S} = i\mathbf{S}$, and $\mathbf{S}^2 = S_x^2 + S_y^2 + S_z^2 = S(S+1)$ with $S = 1$. This model preserves C_4 symmetry represented as

$$C_4 \mathcal{H}(\mathbf{k}) C_4^{-1} = \mathcal{H}(R\mathbf{k}), \quad (3)$$

where $C_4 = e^{-i\pi S_z}$ is a point-group operator for the four-fold rotation about z axis and R is an operator taking (k_x, k_y, k_z) to $(k_y, -k_x, k_z)$. In addition, as $T\mathcal{H}(\mathbf{k})T^{-1} \neq \mathcal{H}(-\mathbf{k})$, where the time-reversal operator $T = \hat{I}\hat{K}$ with $\hat{I} = \text{diag}(1, 1, 1)$ and \hat{K} being the complex conjugate operator, the model does not have time reversal symmetry.

One can find that $\mathcal{H}(\mathbf{k})$ exhibits a threefold degenerate point at $\mathbf{k} = 0$. As shown in Fig. 1(d) with $\beta = 0$, near the degenerate point of the three bands, the dispersions along the k_x and k_y are quadratic while linear along k_z , which is a triple-point with analogous quadratic dispersion of a double Weyl-point. Thus we name such a new triple-point as DTP, which carries a topological charge C that can be defined in terms of the first Chern number on a surface enclosing the point:

$$C_n = \frac{1}{2\pi} \oint_{\mathcal{S}} \mathbf{F}_n(\mathbf{k}) \cdot d\mathcal{S}. \quad (4)$$

Here \mathcal{S} denotes the integration surface, and $\mathbf{F}_n(\mathbf{k}) = \nabla \times \langle u_n(\mathbf{k}) | i\partial_{\mathbf{k}} | u_n(\mathbf{k}) \rangle$ is the Berry curvature of the n -th band with the wave function $|u_n(\mathbf{k})\rangle$, where the band indices n for the lower, middle, and higher bands are

denoted as $-$, 0 , and $+$, respectively. For $\beta = 0$, one has the simple expression $\mathbf{F}_n(\mathbf{k}) = -2n\text{sign}(\alpha)\mathbf{k}/|\mathbf{k}|^3$ and $C_n = -4n\text{sign}(\alpha)$ for the n -th band. Hereafter we use the lower-band Chern number to label the DTPs: $C = C_-$. The simplest DTP in this case with topological charges $C = \pm 4$ is called as type-I DTP. Note that $C_+ = -C_-$ for the higher and lower bands and $C_0 = 0$ for the middle one even if βN_{ij} term exists, which has been numerical confirmed.

Similar to the case for the linear triple-points [26], we find that there are three types of quadratic DTPs induced by the tensors N_{ij} of different forms in Eq. (1). First, the monopole charges of a type-I DTP with $C = \pm 4$ will not change with the three spin-tensors N_{xx} , N_{yy} , and N_{xy} . Second, when $|\beta| > |\alpha| \neq 0$, the tensor N_{zz} induces a DTP with $C = \pm 2$ which is named type-II DTP. Finally, when $|\beta| > 2|\alpha| \neq 0$, a trivial type-III DTP with $C = 0$ can be induced by the tensor N_{xz} or N_{yz} .

Figure 2(a) shows a phase transition between type-I and type-II DTPs which can be induced through the competition between parameters α and β with the spin-tensor $N_{ij} = N_{zz}$ in Eq. (1). In this case, the lowest-band Chern number changes from 4 (type-I) to ± 2 (type-II), and then to -4 (type-I) with decreasing α by fixing $\beta = 1$. As depicted in Figs. 2(b)-(e), the band structure along the $k_x = k_y = 0$ line is concerned. Notably, the Chern number of each band has two contributions from the $k_z > 0$ and $k_z < 0$ branches. For $\alpha > 1$, the $k_z S_z$ term dominates, and the band touching point is still the type-I DTP with $C = 4$ because of the Chern number contributions from the two branches of the lowest band are both $+2$ [Fig. 2(b)]. Decreasing α , the $k_z > 0$ ($k_z < 0$) branch of the lowest band rotates counterclockwise (clockwise). At the critical value $\alpha = 1$, the middle band simultaneously crosses the $k_z > 0$ branch of the lowest band and $k_z < 0$ branch of the higher band. After that, the two branches of lowest band contribute $C_{k_z > 0} = 0$ and $C_{k_z < 0} = 2$, as sketched in Fig. 2(c), give rise to a type-II DTP with $C = 2$, which is consistent with the numerical results in Fig. 2(a). If one further decreases α to 0, another band crossing will occur between the middle band and the $k_z > 0$ ($k_z < 0$) branch of higher (lowest) band [Fig. 2(d)]. However, the DTP is still type-II since this process only changes the sign of C to -2 . The last transition point with level crossing occurs at $\alpha = -1$. Compared with the case $\alpha = 1$, all bands are simply reversed when $\alpha < -1$ as depicted in Fig. 2(e), and the DTP with $C = -4$ belongs to type-I.

The spin-tensors N_{xz} or N_{yz} can induce a type-III DTP with $C = 0$ from a type-I DTP. To illustrate such a phase transition, we choose $N_{ij} = N_{xz}$ with $\alpha = 1$ in Hamiltonian (1). The DTP is of type-I for $|\beta| < 2$ and type-III for $|\beta| > 2$, respectively. At $\beta = 2$, as illustrated in Fig. 2(g), the higher and middle bands cross along two quadratic curves $k_z \pm k_x^2 = k_y = 0$, while the lowest band touches with these two bands at $\mathbf{k} = 0$. Near one of these two curve nodes, e.g., $k_z - k_x^2 = k_y = 0$, the spectra are found to be $\beta k_z/2$ and $(-\beta \pm \sqrt{\beta^2 + 32})k_z/4$. The level

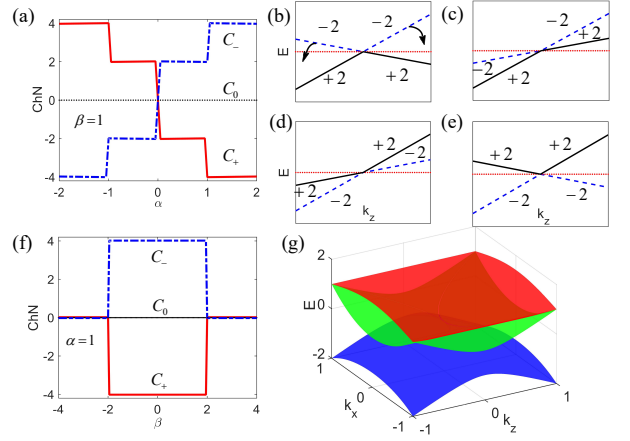


FIG. 2: (Color online). Phase transitions between type-I and type-II (type-III) DTPs by tuning α (β) while fixing $\beta = 1$ ($\alpha = 1$) in Eq. (1). Chern numbers as functions of α (β) for the lowest (dashed blue), middle (dotted black), and higher (solid red) bands are shown in (a) and (f), respectively. (b)-(e) Band structures along the $k_x = k_y = 0$ line with $\alpha = 2, 0.5, -0.5$, and -2 , respectively. The Chern number contributions for each branch are $+2$ (solid black), -2 (dashed blue), and 0 (dotted red). (g) Bands crossing at one of the two transition points with $\beta = 2$, where the lowest, middle, higher bands are labeled by the color blue, green, and red, respectively. The levels crossing only between the middle and higher bands.

crossing in the vicinity of the other curve node is similar. Moreover, for the case of $\beta = -2$, the lowest and middle bands cross along the two curves and the highest band touches with these two bands at $\mathbf{k} = 0$. Because each band crossing changes the Chern number by 2, and the crossings along the two curves are in the same branch, the Chern number must change by 4. Such a topological transition of a DTP from type-I to type-III is shown in Fig. 2(f). In contrast, the Chern number in the transition from type-II to type-III DTPs only changes by 2, and the band crossing is along only one curve. For instance, we consider $\alpha = 1$ and $\beta N_{ij} = c_1 N_{zz} + c_2 N_{xz}$ in the Hamiltonian (1) with $c_{1,2} > 0$, the transition occurs at $c_1 = c_2^2/4 - 1$, and the band crossing is along the $k_x^2 - c_2 k_z/2 = k_y = 0$ curve, as shown in Fig. 3(a).

By introducing a C_4 -breaking term, a quadratic DTP of monopole charge C can be split into two linear triple-points with monopole charge $C/2$. For concreteness, let us consider adding a perturbation term $\lambda^2 S_x$ in the model Hamiltonian (1), then the bands touch at two threefold degenerate points $\mathbf{K}_\pm = (\pm|\lambda|, 0, 0)$. Near these two points, the Hamiltonian can be expanded to the linear order with $\mathbf{q} = \mathbf{k} - \mathbf{K}_\pm$ as

$$\mathcal{H}_\pm(\mathbf{q}) = \mp 2|\lambda|q_x S_x \pm |\lambda|q_y S_y + q_z(\alpha S_z + \beta N_{ij}). \quad (5)$$

A threefold degenerate point described by this effective Hamiltonian is a linear triple point [26]. Specially, the type-I DTP of $C = \pm 4$ for $N_{ij} = N_{zz}$ are broken into two linear triple point with $C = \pm 2$, as shown in Fig. 3(b). The effects of C_4 -breaking terms for type-II and

type-III are similar.

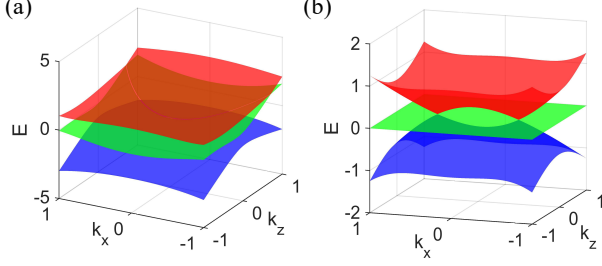


FIG. 3: (Color online). (a) Bands crossing at the transition point for $\alpha = 1$ and $\beta N_{ij} = c_1 N_{zz} + c_2 N_{xx}$ in the Hamiltonian (1) with $c_1 = 1$ and $c_2 = 2\sqrt{2}$. The levels crossing only between the middle and highest bands along one quadratic curve at the $k_z > 0$ branch. (b) For $\alpha = 1$ and $\beta = 0$, a quadratic type-I DTP ($C = \pm 4$) splits into two linear TPs carrying the same monopole ($C = \pm 2$).

III. DTP FERMIONS IN 2D LATTICE MODEL

For a lattice system that is filled with fermionic particles and effectively described by the low-energy Hamiltonian (1), the quasiparticle excitations near the DTPs can be named DTP fermions with (pseudo)spin-1 and quadratic dispersion. In this section, we first study DTP fermions in a 2D lattice model, which can reduce into the Hamiltonian (1) without k_z terms. The three spin-1 states are labeled as $|\uparrow\rangle$, $|0\rangle$, $|\downarrow\rangle$, and the 2D tight-binding Hamiltonian on a square lattice is given by

$$\begin{aligned}\hat{H}_{2D} &= t \sum_{\mathbf{r}} [\hat{H}_{\mathbf{rx}} + \hat{H}_{\mathbf{ry}} + \hat{H}_{\mathbf{rxy}} + \hat{H}_{\mathbf{M}}], \\ \hat{H}_{\mathbf{rx}} &= \left[-\frac{i}{2} (\hat{a}_{\mathbf{r},0}^\dagger \hat{a}_{\mathbf{r}+\mathbf{x},\uparrow} + \hat{a}_{\mathbf{r},0}^\dagger \hat{a}_{\mathbf{r}-\mathbf{x},\uparrow}) + \text{H.c.} \right] \\ &\quad + \left[\frac{i}{2} (\hat{a}_{\mathbf{r},\downarrow}^\dagger \hat{a}_{\mathbf{r}+\mathbf{x},0} + \hat{a}_{\mathbf{r},\downarrow}^\dagger \hat{a}_{\mathbf{r}-\mathbf{x},0}) + \text{H.c.} \right], \\ \hat{H}_{\mathbf{ry}} &= \left[-\frac{i}{2} (\hat{a}_{\mathbf{r},0}^\dagger \hat{a}_{\mathbf{r}+\mathbf{y},\uparrow} + \hat{a}_{\mathbf{r},0}^\dagger \hat{a}_{\mathbf{r}-\mathbf{y},\uparrow}) + \text{H.c.} \right] \\ &\quad + \left[\frac{i}{2} (\hat{a}_{\mathbf{r},\downarrow}^\dagger \hat{a}_{\mathbf{r}+\mathbf{y},0} + \hat{a}_{\mathbf{r},\downarrow}^\dagger \hat{a}_{\mathbf{r}-\mathbf{y},0}) + \text{H.c.} \right], \\ \hat{H}_{\mathbf{rxy}} &= \left[-\frac{i}{4} (\hat{a}_{\mathbf{r},\downarrow}^\dagger \hat{a}_{\mathbf{r}+(\mathbf{x}-\mathbf{y}),\uparrow} + \hat{a}_{\mathbf{r},\downarrow}^\dagger \hat{a}_{\mathbf{r}-(\mathbf{x}-\mathbf{y}),\uparrow}) + \text{H.c.} \right] \\ &\quad + \left[\frac{i}{4} (\hat{a}_{\mathbf{r},\downarrow}^\dagger \hat{a}_{\mathbf{r}+(\mathbf{x}+\mathbf{y}),\uparrow} + \hat{a}_{\mathbf{r},\downarrow}^\dagger \hat{a}_{\mathbf{r}-(\mathbf{x}+\mathbf{y}),\uparrow}) + \text{H.c.} \right], \\ \hat{H}_{\mathbf{M}} &= iM \hat{a}_{\mathbf{r},0}^\dagger \hat{a}_{\mathbf{r},\uparrow} + \text{H.c.},\end{aligned}\tag{6}$$

where $\hat{a}_{\mathbf{r},s}$ ($\hat{a}_{\mathbf{r},s}^\dagger$) is the annihilation (creation) operator on site \mathbf{r} with spin $s = \{\uparrow, 0, \downarrow\}$, M is the strength of an effective Zeeman potential, and the hopping strength is set $t = 1$ as the energy unit hereafter. The terms $\hat{H}_{\mathbf{rx}}$, $\hat{H}_{\mathbf{ry}}$, and $\hat{H}_{\mathbf{rxy}}$ represent the spin-flip hopping along

x , y , and $x \pm y$ axis, respectively. Under the periodic boundary condition, the tight-binding Hamiltonian can be written as $\hat{H}_{2D} = \sum_{\mathbf{k}, s, s'} \hat{a}_{\mathbf{k}s}^\dagger [\mathcal{H}(\mathbf{k})]_{ss'} \hat{a}_{\mathbf{k}s'}$, where $\hat{a}_{\mathbf{k}s} = 1/\sqrt{V} \sum_{\mathbf{r}} e^{-i\mathbf{k}\cdot\mathbf{r}} \hat{a}_{\mathbf{r}s}$ is the annihilation operator in momentum space $\mathbf{k} = (k_x, k_y)$, and the Bloch Hamiltonian is written as (the lattice spacing $a \equiv 1$ and $\hbar \equiv 1$)

$$\begin{aligned}\mathcal{H}(\mathbf{k}) &= \mathbf{d}(\mathbf{k}) \cdot \mathbf{S}, \\ d_x &= \cos k_x - \cos k_y, \\ d_y &= \sin k_x \sin k_y, \\ d_z &= M - \cos k_x - \cos k_y.\end{aligned}\tag{7}$$

The energy spectrum is given by $E(\mathbf{k}) = 0, \pm|\mathbf{d}(\mathbf{k})|$, which contains a zero-energy flat band in the middle of the three bands. For $M = 2$ ($M = -2$), the three bands touch at a single point $\mathbf{K}_+ = (0, 0)$ [$\mathbf{K}_- = (\pi, \pi)$] in the first Brillouin zone, as shown in Fig. 4(a). Expanding the Bloch Hamiltonian near the threefold degenerate point with $\mathbf{q} = \mathbf{k} - \mathbf{K}_\pm$ yields the low-energy effective Hamiltonian

$$\mathcal{H}_{\text{eff}}^\pm(\mathbf{q}) = \pm \left[\frac{1}{2} (q_y^2 - q_x^2) S_x + q_x q_y S_y \right],\tag{8}$$

indicating that this threefold degenerate point is a 2D DTP with quadratic dispersion along k_x and k_y directions. When the Fermi level lies near the 2D DTP, the lattice system is in a metallic phase with emergent 2D DTP fermions.

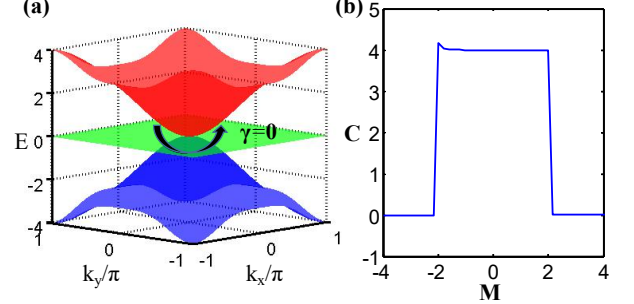


FIG. 4: (Color online) (a) The band dispersion in the $k_x - k_y$ plane with $M = 2$. (b) The Chern numbers as a function of M . When $M \neq \pm 2$, the 2D system is in the topological or trivial insulating phase.

To further study the topological properties of the system, we first calculate the Berry phase of the 2D DTP point for $M = \pm 2$ by circling around it

$$\gamma = \oint_C d\mathbf{k} \cdot \mathbf{A}(\mathbf{k}),\tag{9}$$

where the Berry connection $\mathbf{A}(\mathbf{k}) = i\langle u_-(\mathbf{k}) | \nabla_{\mathbf{k}} | u_-(\mathbf{k}) \rangle$. The analytical calculation gives the Berry phase $\gamma = 0$ for both $M = \pm 2$ which is confirmed by numerical integration. Thus, the 2D DTPs are topologically trivial, and the 2D DTP fermions in this model are not topological quasiparticles. When $M \neq \pm 2$, the system changes

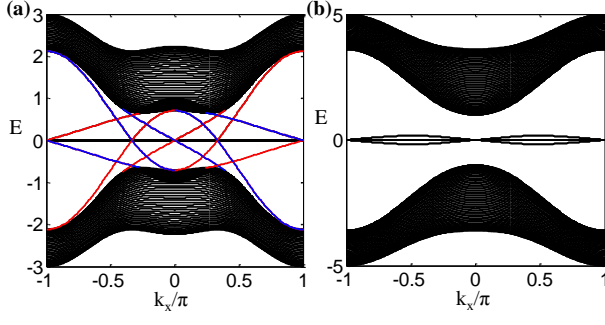


FIG. 5: (Color online) (a) The energy spectrum $E(k_x)$ of reduced chain with lattice sites $L_y = 60$ under open boundaries for (a) $M = 1$ and (b) $M = 3$. The red and blue colors denote the edge modes in opposite edges.

from a trivial metallic state to an insulator state with band gaps. We then calculate the Chern number of the lowest gapped band

$$C = \frac{1}{2\pi} \int_{\text{BZ}} dk_x dk_y \frac{1}{d^3} \mathbf{d} \cdot (\partial_{k_x} \mathbf{d} \times \partial_{k_y} \mathbf{d}). \quad (10)$$

The obtained C as a function of the parameter M is shown in Fig. 4(b), which indicates that the system is a topological Chern (trivial band) insulator with $C = 4$ ($C = 0$) when $|M| < 2$ ($|M| > 2$). We also numerically calculate the energy spectrum $E(k_x)$ under open boundary condition along y direction with the lattice length $L_y = 60$ for fixed $M = 1$ and $M = 3$, respectively. As shown in Figs. 5(a) and (b) for $M = 1$ and $M = 3$, there are four and zero chiral in-gap edge states connecting the three bulk bands, which is consistent of the bulk-edge correspondence for $C = 4$ and $C = 0$, respectively.

IV. DTP FERMIONS IN 3D LATTICE MODEL

We proceed to study the DTP fermions in a 3D cubic lattice system, which can reduce into the Hamiltonian (1). The corresponding 3D tight-binding Hamiltonian is given by

$$\begin{aligned} \hat{H}_{3D} &= \hat{H}_{2D} + \sum_{\mathbf{r}} \hat{H}_{\mathbf{r}z}, \\ \hat{H}_{\mathbf{r}z} &= -\frac{i\alpha}{2} (\hat{a}_{\mathbf{r},0}^\dagger \hat{a}_{\mathbf{r}+\mathbf{z},\uparrow} + \hat{a}_{\mathbf{r},0}^\dagger \hat{a}_{\mathbf{r}-\mathbf{z},\uparrow}) + \text{H.c.}, \end{aligned} \quad (11)$$

where $\hat{H}_{\mathbf{r}z}$ denotes the hopping term along the z axis. The Bloch Hamiltonian of the 3D system for $\alpha = 1$ takes the form as

$$\begin{aligned} \mathcal{H}(\mathbf{k}) &= (\cos k_x - \cos k_y) S_x + \sin k_x \sin k_y S_y \\ &+ (M - \cos k_x - \cos k_y - \cos k_z) S_z. \end{aligned} \quad (12)$$

There are a pair of threefold degenerate points in the energy bands located at $\mathbf{T}_1^\pm = [0, 0, \pm \arccos(M-2)]$ for $1 < M < 3$ as shown in Fig. 6(a), and another pair at

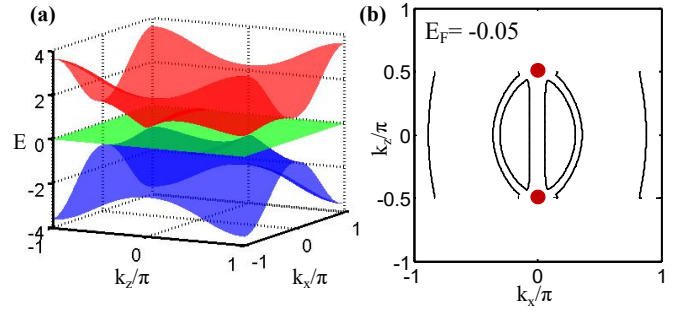


FIG. 6: (Color online) (a) The band dispersion as a function of k_x and k_z for $k_y = 0$ and $M = 2$. (b) The Fermi arcs appear at $E_F = -0.05$ under the open boundary condition along the y direction. The black lines denote the surface states, and the two red dots denote the position of DTPs.

$\mathbf{T}_2^\pm = [\pi, \pi, \pm \arccos(M+2)]$ for $-3 < M < -1$. One can obtain the low-energy effective Hamiltonian around \mathbf{T}_1^\pm with $\mathbf{q} = \mathbf{k} - \mathbf{T}_1^\pm$:

$$\mathcal{H}_{\text{eff}}^\pm(\mathbf{q}) = \frac{1}{2} (q_y^2 - q_x^2) S_x + q_x q_y S_y \pm v_z q_z S_z, \quad (13)$$

where $v_z = \sqrt{1 - (M-2)^2}$ for $1 < M < 3$. The monopole charge of the DTPs \mathbf{T}_1^\pm can be obtained as $C = \pm 4$, then they are type-I DTPs (\mathbf{T}_2^\pm are also type-I DTPs). Since the 3D bulk bands are fully gapped when $k_z \neq \pm k_z^c$ with $k_z^c = \arccos(M-2)$, considering k_z as a good quantum number, the dimension reduction Hamiltonian $\mathcal{H}_{k_z}(k_x, k_y)$ for a fixed $k_z \neq \pm k_z^c$ can be viewed as a 2D Chern insulator, which is topologically characterized by the k_z -dependent Chern number defined on the k_x - k_y plane [see Eq. (10)]:

$$C_{k_z} = \begin{cases} 0, & |k_z| > k_z^c; \\ 4, & 0 < |k_z| < k_z^c. \end{cases} \quad (14)$$

Thus the type-I DTPs with monopole charge $C = \pm 4$ act as the topological transition points between two layer topological insulators with Chern number difference $\Delta C_{k_z} = \pm 4 = C$. Using open boundary condition along y direction, we find that there are four Fermi arcs surface states effectively connecting the pair of DTPs, as shown in Fig. 6(b). In these cases, the system has the topological metal bands with emergent DTP fermions. At the critical points $M = \pm 1$ or ± 3 , the two DTPs merge and then disappear by opening a gap when $|M| < 1$ and $|M| > 3$. For $|M| < 1$, the system is in a weak topological insulator phase, which has the Chern number $C_{k_z} = 4$ for all k_z and chiral surface states under open boundary condition. For $|M| > 3$, it is a trivial insulating phase.

To further study the C_4 -symmetry breaking effect, we add a term $\mathcal{H}_p = \delta S_x$ to the Bloch Hamiltonian in Eq. (12), which corresponds to the in-site coupling described by the lattice Hamiltonian $\hat{H}_p = i\delta \sum_{\mathbf{r}} \hat{a}_{\mathbf{r},\uparrow}^\dagger \hat{a}_{\mathbf{r},0} + \text{H.c.}$. Under the symmetry breaking perturbation, each quadratic DTP splits into two linear triple points. By

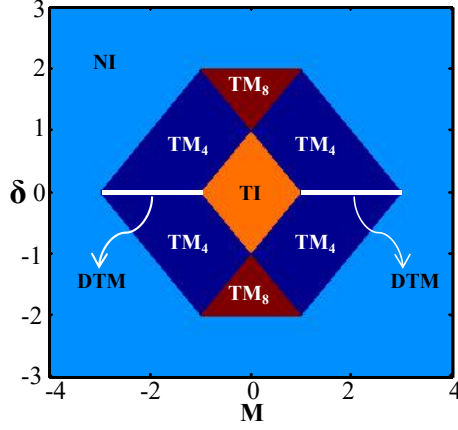


FIG. 7: (Color online) The phase diagram of the 3D lattice system with a C_4 -symmetry breaking term. DTM denotes the DTP metal phase (white lines), TI (orange) and NI (light blue) denote a weak topological and normal insulating phase, TM_4 (dark blue) and TM_8 (red) represent the triple-point metal phase with four and eight triple points, respectively.

varying the parameters M and δ , we can obtain the phase diagram of the 3D lattice system, as shown in Fig. 7. In the phase diagram, apart from a normal band insulating phase (denoted by NI) with $C_{k_z} = 0$ and a weak topological insulating phase (denoted by TI) with $C_{k_z} = 4$ for all range of k_z , there are another three different phases: the DTP metal phase (denoted by DTM), the triple-point metal phase with four triple points (denoted by TM_4) and triple-point metal phase with eight triple points (denoted by TM_8). For example, for $0 < \delta < 2$ and $1 - M < \delta < 3 - M$, the four triple points are located at $(k_x, k_y, k_z) = (-\arccos(1 - \delta), 0, \pm \arccos(M - 2 + \delta))$ and $(\arccos(1 - \delta), 0, \pm \arccos(M - 2 + \delta))$. For the TM_8 phase when $1 < \delta < 2$, the eight triple points are located at $(-\arccos(1 - \delta), 0, \pm \arccos(M - 2 + \delta))$, $(\arccos(1 - \delta), 0, \pm \arccos(M - 2 + \delta))$, $(\pi, -\arccos(\delta - 1), \pm \arccos(M + 2 - \delta))$, and $(\pi, \arccos(\delta - 1), \pm \arccos(M + 2 - \delta))$.

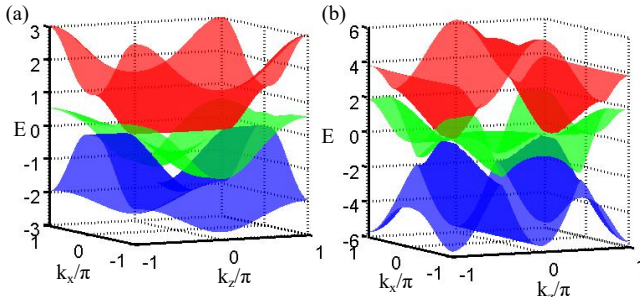


FIG. 8: (Color online) (a) The energy band in the k_x - k_z plane with $k_y = 0$: (a) type-II DTPs for $\alpha = 0.5$, $\beta = 1$ and $M = 1.8$; (b) type-III DTPs for $\alpha = 1$, $\beta = 3$ and $M = 1.8$.

As analyzed in Sec. II, we can add an additional spin-tensor term to induce the phase transition between type-I and type-II DTPs. The required spin-tensor term

$v_z k_z N_{zz}$ (let $\beta = 1$) in the continuum Hamiltonian (1) corresponding to the lattice Hamiltonian

$$\begin{aligned} \hat{H}_{zz} &= \sum_{\mathbf{r}} \hat{H}_{\mathbf{r}zz} + \hat{H}_{\mathbf{M}zz}, \\ \hat{H}_{\mathbf{r}zz} &= -\frac{1}{2}(\hat{a}_{\mathbf{r},\uparrow}^\dagger \hat{a}_{\mathbf{r}+\mathbf{z},\uparrow} + \hat{a}_{\mathbf{r},0}^\dagger \hat{a}_{\mathbf{r}+\mathbf{z},0}) + \text{H.c.}, \\ \hat{H}_{\mathbf{M}zz} &= (M-2)\hat{a}_{\mathbf{r},\uparrow}^\dagger \hat{a}_{\mathbf{r},\uparrow} + \hat{a}_{\mathbf{r},0}^\dagger \hat{a}_{\mathbf{r},0}. \end{aligned} \quad (15)$$

In this case when $1 < M < 3$ and $0 < |\alpha| < 1$, there are a pair of type-II DTPs at $(0, 0, \pm k_z^c)$ in the first Brillouin zone, as shown in Fig. 8(a) with the energy bands. For the 3D lattice system with the type-II DTPs, we obtain the k_z -dependent Chern number for the lowest band

$$C_{k_z} = \text{sign}(\alpha) \times \begin{cases} 2, & |k_z| > k_z^c; \\ 4, & 0 < |k_z| < k_z^c. \end{cases} \quad (16)$$

The type-II DTPs with monopole charges ± 2 also act as the transition points between two layer topological insulators with Chern number difference $\Delta C_{k_z} = \pm 2$.

To induce the transition from type-I to type-III DTPs, the required spin-tensor term $\beta v_z k_z N_{xz}$ in Hamiltonian (1) takes the following form of lattice Hamiltonian

$$\begin{aligned} \hat{H}_{xz} &= \sum_{\mathbf{r}} \hat{H}_{\mathbf{r}xz} + \hat{H}_{\mathbf{M}xz}, \\ \hat{H}_{\mathbf{r}xz} &= \frac{\beta}{4}(\hat{a}_{\mathbf{r},\downarrow}^\dagger \hat{a}_{\mathbf{r}+\mathbf{z},\uparrow} + \hat{a}_{\mathbf{r},\downarrow}^\dagger \hat{a}_{\mathbf{r}-\mathbf{z},\uparrow}) + \text{H.c.}, \\ \hat{H}_{\mathbf{M}xz} &= -\frac{\beta(M-2)}{2}(\hat{a}_{\mathbf{r},\downarrow}^\dagger \hat{a}_{\mathbf{r},\uparrow} + \hat{a}_{\mathbf{r},\uparrow}^\dagger \hat{a}_{\mathbf{r},\downarrow}). \end{aligned} \quad (17)$$

With this addition spin-tensor term, when $1 < M < 3$ and $|\beta| > 2$ ($\alpha = 1$), there are a pair of type-III DTPs at $(0, 0, \pm k_z^c)$ in the first Brillouin zone, as shown in Fig. 8(b) with the energy bands. For the 3D lattice system with the trivial type-III DTPs, the k_z -dependent Chern number $C_{k_z} = 0$ for all k_z .

V. REALIZATION AND DETECTION IN OPTICAL LATTICES

In this section, we discuss the realization of the lattice models and detection of the topological properties of the emergent DTP fermions in optical lattices. We consider a noninteracting degenerate fermionic gas in a 3D cubic (or 2D square) optical lattice, and the three spin states $|\uparrow\rangle$, $|0\rangle$, $|\downarrow\rangle$ are encoded by three atomic internal states. By defining the three-component annihilation operator at site \mathbf{r} as $\hat{\mathbf{a}}_{\mathbf{r}} = (\hat{a}_{\mathbf{r},\uparrow}, \hat{a}_{\mathbf{r},0}, \hat{a}_{\mathbf{r},\downarrow})^T$, the 3D lattice Hamiltonian in Eq. (11) can be rewritten as

$$\begin{aligned} \hat{H}_{3D} &= \sum_{\mathbf{r}, \eta} \left(\hat{a}_{\mathbf{r}+\boldsymbol{\eta}}^\dagger U_\eta \hat{\mathbf{a}}_{\mathbf{r}} + \text{H.c.} \right) + M \sum_{\mathbf{r}} \hat{a}_{\mathbf{r}}^\dagger S_z \hat{\mathbf{a}}_{\mathbf{r}} \\ &\quad + \sum_{\mathbf{r}} \left[\hat{a}_{\mathbf{r}+(\mathbf{x}+\mathbf{y})}^\dagger U_{xy} \hat{\mathbf{a}}_{\mathbf{r}} - \hat{a}_{\mathbf{r}+(\mathbf{x}-\mathbf{y})}^\dagger U_{xy} \hat{\mathbf{a}}_{\mathbf{r}} + \text{H.c.} \right], \end{aligned} \quad (18)$$

where $\eta = x, y, z$ denote the hopping directions. The hopping matrices along the three axis and xy direction are given by $U_x = \frac{1}{2}(S_x - S_z)$, $U_y = -\frac{1}{2}(S_x + S_z)$, $U_z = -\frac{1}{2}S_z$, and $U_{xy} = -\frac{1}{4}S_y$, respectively. For a square lattice without the U_z term, the Hamiltonian recovers to the 2D model in Eq. (6).

The terms U_η and U_{xy} describe atomic hopping between two lattice sites with spin flipping, which can be achieved by the laser-assisted tunnelling technique with well-designed Raman coupling between the two spin states [29–33]. In experiments, one can first use a moderate magnetic field to distinguish the spin states, and then the natural hopping t_N along each direction is suppressed by titling the cubic optical lattice with a homogeneous energy gradient along the η direction, with the large tilt potential $\Delta_\eta \gg t_N$. The tilt potential can be created through the natural gravitational field or the gradient of a dc- or ac-Stark shift. In order to distinguish the tunnellings directed along different directions for independent Raman coupling, one requires different linear energy shifts per site $\Delta_x \neq \Delta_y \neq \Delta_z \neq \Delta_x \pm \Delta_y$. Finally, the hopping terms can be restored and engineered by application of two-photon Raman coupling with the laser beams of proper configurations through the laser-frequency and polarization selections [29–32]. The spin-tensor terms in Eqs. (15) and (17) can also be engineered in this way. In principle, arbitrary hopping matrices including the required hopping terms can be independently created with well-designed laser configurations [29–32]. Particularly, the detailed Raman-coupling schemes have been proposed to realize similar hopping terms with spin flip $S_{x,y,z}$ for cold atoms in a 3D cubic lattice [24, 26, 71]. We note that the realization of all the hopping terms is technically extremely challenging since a considerable number of Raman beams are needed. Although the beams can be drawn from the same laser by an electric or acoustic optical modulator, one should overcome the difficulties in the implementation of the Raman lasers that are associated with the heating for the required spin-changing transitions.

To detect the emergent DTP quasiparticles in the optical lattice, one can first detect the DTP as the band crossings. The 2D and 3D DTPs can be probed via the Bragg spectroscopy or Bloch-Zener oscillations from measuring the atomic zener tunneling to excited band after a Bloch oscillation, similar to the methods used for detecting Dirac points [35–37] and Weyl points [60, 62, 67] in optical lattices. The Berry phase of a 2D DTP can be directly measured using an interferometric approach in momentum space [38]. Moreover, it has been demonstrated that the full tomography of Bloch states (vectors) can be achieved with cold atoms in optical lattices to reveal the band topology [72–77], which would be applicable in our proposed system.

For the 3D case, we show that the k_z -dependent Chern number C_{k_z} can also be measured from the shift of the hybrid Wannier center of an atomic cloud, based on the particle pumping approach and hybrid Wannier functions

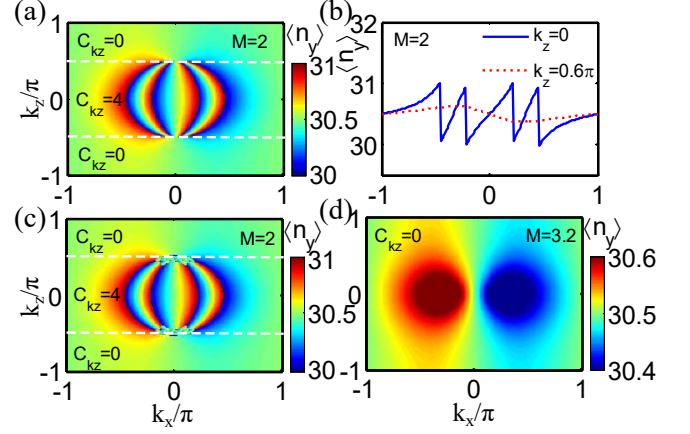


FIG. 9: (Color online) The hybrid Wannier center $\langle n_y(k_x, k_z) \rangle$ in a tight-binding chain of length $L_y = 60$ under the open boundary condition at 1/3 filling (the particle number of the three-component fermionic atoms is fixed as $N_a = L_y = 60$ in numerical simulations) as a function of the adiabatic pumping parameter k_x for different k_z . (a) The profile $\langle n_y(k_x, k_z) \rangle$ for $M = 2$ without trapping potential shows four jumps of one-unit-cell for k_z within the region $(-0.5\pi, 0.5\pi)$, with typical examples shown in (b). (c) The profile $\langle n_y(k_x, k_z) \rangle$ for $M = 2$ under a weak harmonic trap with $V_t = 2 \times 10^{-4}t$ ($t = 1$ as the energy unit). (d) The profile $\langle n_y(k_x, k_z) \rangle$ without trapping potential for $M = 3.2$ shows the absence of one-unit-cell jumps for all k_z in the topologically trivial regime.

in band theory [48–52, 78–80]. For a fixed k_z ($k_z \neq k_z^c$), the Hamiltonian $H_{k_z}(k_x, k_y)$ describes a 2D insulating lattice system, which can be viewed as a fictitious 1D insulator along y , subject to the external parameter k_x and k_z . The polarization of this 1D insulator can be defined by means of hybrid Wannier functions [78–80], which are localized in the y axis retaining Bloch character along k_x and k_z . When k_x is adiabatically changed by 2π , the change in polarization, i.e., the shift of the hybrid Wannier center, is proportional to the k_z -dependent Chern number, which is a manifestation of topological pumping with k_x being the adiabatic pumping parameter. Considering the Bloch Hamiltonian in Eq. (12) with parameters k_x and k_z , and transforming it to the tight-binding Hamiltonian along the y axis, we can construct the hybrid Wannier center as [67, 78]

$$\langle n_y(k_x, k_z) \rangle = \frac{\sum_{i_y} i_y \rho_{i_y}(k_x, k_z)}{\sum_{i_y} \rho_{i_y}(k_x, k_z)}, \quad (19)$$

where $\rho_{i_y}(k_x, k_z)$ is the density of the hybrid Wannier function as a function of k_x and k_z , with i_y being the lattice-site index in the 1D tight-binding chain. Here, the hybrid density can be written as

$$\rho_{i_y}(k_x, k_z) = \sum_{\text{occ}} |k_x, k_z\rangle_{i_y} \langle k_x, k_z|, \quad (20)$$

where $|k_x, k_z\rangle_{i_y}$ denotes the hybrid wave function of the system at site i_y and notation occ denotes the occupied

states. Experimentally, the atomic density $\rho_{i_y}(k_x, k_z)$ can be directly detected by the hybrid time-of-flight images [78], combining *in situ* imaging along y and time-of-flight imaging along the release directions x and z . In the measurement, the optical lattice is switched off along x and z , while the system remains unchanged along y . Thus, one can directly extract C_{k_z} from an experimental detection of the shift in the hybrid function center.

We numerically calculate $\langle n_y(k_x, k_z) \rangle$ from Eq. (19) in a 1D reduced tight-binding chain of length $L_y = 60$ at $1/3$ filling (the lowest band is filled), with typical results shown in Fig. 9. Here we note that for three-component fermionic atoms in the three-band model with the total lattice site N_L , the particle number is $N_a = N_L$ (the average atomic density is 1) under the $1/3$ filling condition. In our numerical simulation for the reduced 1D chain with parameters k_x and k_z , the fermion number is thus fixed as $N_a = L_y = 60$ for various k_x and k_z . To consider the effect of the fluctuations of $\rho_{i_y}(k_x, k_z)$ in realistic experiments, we simply add local fluctuations as $(1 + w_{i_y})\rho_{i_y}(k_x, k_z)$ in our numerical calculations, where the random parameter w_{i_y} for the site i_y is uniformly distributed in the range $[-W, W]$ with the fluctuation strength W . We have numerically checked that the results of $\langle n_y(k_x, k_z) \rangle$ shown in Fig. 9 can preserve when the fluctuation strength $W \lesssim 30\%$ ($W \lesssim 5\%$) for the quantity averaged over hundreds of random samplings (a single random sampling). Thus, such a magnitude of the density fluctuations would not affect the measurements in practical cold-atom experiments after averaging the samples.

For the case of $M = 2$ in Figs. 9(a) and (b), the results show that the system exhibits four discontinuous jumps of one unit cell within the region $k_z \in (-k_z^c, k_z^c)$ with $k_z^c = 0.5\pi$, as k_x changing from $-\pi$ to π . This indicates that when $k_z \in (-k_z^c, k_z^c)$, $C_{k_z} = 4$ and outside this region $C_{k_z} = 0$. For $M = 3.2$ in Fig. 9(d), there is no discontinuous jump in $\langle n_y(k_x, k_z) \rangle$, which indicates that the system is in the trivial insulator phase with $C_{k_z} = 0$ for all k_z . To take the realistic experiment into account, we add a weak harmonic trap $\hat{H}_t = V_t \sum_n (n - \frac{L_y}{2})^2 \hat{a}_n^\dagger \hat{a}_n$ to this finite-site lattice, where V_t is the trap strength. Within a local-density approximation, the lowest band is still filled at the center of the trap and thus the shift of the

hybrid Wannier center is expected to be nearly the same as those without the trap potential. When the band gap $E_g \leq V_t(i_y - \frac{L_y}{2})^2$, the lowest band is only partially filled near the two edges and then this pumping argument does not apply to this region. With numerical simulations shown in Fig. 9(c), $\langle n_y(k_x, k_z) \rangle$ preserve with a deviation less than 2% except the regions near the DTPs for $V_t = 2 \times 10^{-4}t$, which are consistent with the estimations in the local-density analysis.

VI. CONCLUSIONS

In summary, we have proposed a class of pseudospin-1 quadratic DTP fermions emerging in topological metal bands. We have analyzed a general three-band continuum model with C_4 symmetry in three dimensions, which has three types of threefold DTPs as spin-1 generalization of double-Weyl points, classified by their topological charges. The 2D and 3D tight-binding lattice models of topological metal bands with exotic DTP fermions near the DTPs have also been proposed and explored. In 2D, the bands close at a trivial DTP with zero Berry phase, which occurs at the transition between the normal and topological insulator phases. In 3D, the topological properties of three different DTP fermions in lattice systems are further investigated, and the effects of breaking C_4 symmetry are also considered, which generally leads to splitting each quadratic DTP into two linear triple points and gives topological phase diagrams. Finally, we have discussed realization of the proposed models and detection of the topological properties of the DTP fermions in optical lattices.

Acknowledgments

This work was supported by the NSFC (Grant No. 11604103, No. 11704132, No. 11474153, and No. 91636218), the NKRD of China (Grant No. 2016YFA0301803), the NSAF (Grant No. U1830111), the NSF of Guangdong Province (Grant No. 2016A030313436), the Startup Foundation of SCNU, and the Innovation project of Graduate School of SCNU.

-
- [1] N. Armitage, E. Mele, and A. Vishwanath, Weyl and Dirac Semimetals in three-dimensional solids, *Rev. Mod. Phys.* **90**, 015001 (2018).
 - [2] X. Wan, A. M. Turner, A. Vishwanath, and S. Y. Savrasov, Topological semimetal and Fermi-arc surface states in the electronic structure of pyrochlore iridates, *Phys. Rev. B* **83**, 205101 (2011).
 - [3] A. A. Burkov, M. D. Hook, and L. Balents, Topological nodal semimetals, *Phys. Rev. B* **84**, 235126 (2011).
 - [4] L. Balents, Weyl electrons kiss, *Physics* **4**, 36 (2011).
 - [5] A. A. Burkov and L. Balents, Weyl Semimetal in a

- Topological Insulator Multilayer, *Phys. Rev. Lett.* **107**, 127205 (2011).
- [6] A. A. Zyuzin and A. A. Burkov, Topological response in Weyl semimetals and the chiral anomaly, *Phys. Rev. B* **86**, 115133 (2012).
- [7] S. A. Parameswaran, T. Grover, D. A. Abanin, D. A. Pesin, and A. Vishwanath, Probing the Chiral Anomaly with Nonlocal Transport in Three-Dimensional Topological Semimetals, *Phys. Rev. X* **4**, 031035 (2014).
- [8] C. Fang, L. Lu, J. Liu, and L. Fu, Topological semimetals with Riemann surface state, *Nat. Phys.* **12**, 936 (2016).

- [9] S.-Y. Xu, I. Belopolski, N. Alidoust, M. Neupane, C. Zhang, R. Sankar, S.-M. Huang, C.-C. Lee, G. Chang, B. Wang, G. Bian, H. Zheng, D. S. Sanchez, F. Chou, H. Lin, S. Jia, and M. Z. Hasan, Discovery of a Weyl fermion semimetal and topological Fermi arcs, *Science* **349**, 613 (2015).
- [10] B. Q. Lv, H. M. Weng, B. B. Fu, X. P. Wang, H. Miao, J. Ma, P. Richard, X. C. Huang, L. X. Zhao, G. F. Chen, Z. Fang, X. Dai, T. Qian, H. Ding Experimental discovery of Weyl semimetal TaAs, *Phys. Rev. X* **5**, 031013 (2015).
- [11] G. Xu, H. Weng, Z. Wang, X. Dai, and Z. Fang, Chern Semimetal and the Quantized Anomalous Hall Effect in HgCr_2Se_4 , *Phys. Rev. Lett.* **107**, 186806 (2011).
- [12] C. Fang, M. J. Gilbert, X. Dai, and B. A. Bernevig, Multi-Weyl Topological Semimetals Stabilized by point Group Symmetry, *Phys. Rev. Lett.* **108**, 266802 (2012).
- [13] S.-M. Huang, S.-Y. Xu, I. Belopolski, C.-C. Lee, G. Chang, T.-R. Chang, B. Wang, N. Alidoust, G. Bian, M. Neupane, D. Sanchez, H. Zheng, H.-T. Jeng, A. Bansil, T. Neupert, H. Lin, and M. Z. Hasan, New type of Weyl semimetal with quadratic double Weyl fermions, *Proc. Natl. Acad. Sci. USA* **113**, 1180 (2016).
- [14] B. Bradlyn, J. Cano, Z. Wang, M. G. Vergniory, C. Felser, R. J. Cava, and B. A. Bernevig, Beyond Dirac and Weyl fermions: Unconventional quasiparticles in conventional crystals, *Science* **353**, 5037 (2016).
- [15] B. Q. Lv, et al. Observation of three-component fermions in the topological semimetal molybdenum phosphide. *Nature (London)* **546**, 627 (2016).
- [16] B. J. Wieder, Y. Kim, A. M. Rappe, and C. L. Kane, Double Dirac Semimetals in Three dimensions, *Phys. Rev. Lett.* **116**, 186402 (2016).
- [17] H. Weng, C. Fang, Z. Fang, and X. Dai, Topological Semimetals with Triply Degenerate Nodal Points in θ -phase Tantalum Nitride, *Phys. Rev. B* **93**, 241202 (2016).
- [18] Z. Zhu, G. W. Winkler, Q. S. Wu, J. Li, and A. A. Soluyanov, Triple point Topological Metals, *Phys. Rev. X* **6**, 031003 (2016).
- [19] G. Chang, S. Y. Xu, B. J. Wieder, D. S. Sanchez, S. M. Huang, I. Belopolski, T. R. Chang, S. Zhang, A. Bansil, H. Lin, and M. Zahid, Unconventional Chiral Fermions and Large Topological Fermi Arcs in RhSi , *Phys. Rev. Lett.* **119**, 206401 (2017).
- [20] P. Tang, Q. Zhou, and S. C. Zhang, Multiple Types of Topological Fermions in Transition Metal Silicides, *Phys. Rev. Lett.* **119**, 206402 (2017).
- [21] I. C. Fulga and A. Stern, Triple point fermions in a minimal symmorphic model, *Phys. Rev. B* **95**, 241116(R) (2017).
- [22] Y. Xu, L. M. Duan, Unconventional quantum Hall effects in two-dimensional massive spin-1 fermion systems, *Phys. Rev. B* **96**, 155301 (2017).
- [23] J.-Z. Ma, et al. Three-component fermions with surface Fermi arcs in tungsten carbide, *Nat. Phys.* **14**, 349 (2018).
- [24] Y.-Q. Zhu, D.-W. Zhang, H. Yan, D. Y. Xing, S.-L. Zhu, Emergent pseudospin-1 Maxwell fermions with a threefold degeneracy in optical lattices, *Phys. Rev. A* **96**, 033634 (2017).
- [25] I. C. Fulga, L. Fallani, and M. Burrello, Geometrically protected triple-point crossings in an optical lattice, *Phys. Rev. B* **97**, 121402(R) (2018).
- [26] H. Hu, J. Hou, F. Zhang, and C. Zhang, Topological Triply-Degenerate Points Induced by Spin-Tensor-Momentum Couplings, *Phys. Rev. Lett.* **120**, 240401 (2018).
- [27] Z. Lan, N. Goldman, A. Bermudez, W. Lu, and P. Öhberg, Dirac-Weyl fermions with arbitrary spin in two-dimensional optical superlattices, *Phys. Rev. B* **84**, 165115 (2011).
- [28] L. Liang and Y. Yu, Rarita-Schwinger-Weyl semimetal in $J_{\text{eff}}=3/2$ electron systems, *Phys. Rev. B* **93**, 045113 (2016).
- [29] J. Dalibard, F. Gerbier, G. Juzeliūnas, and P. Öhberg, Colloquium: Artificial gauge potentials for neutral atoms, *Rev. Mod. Phys.* **83**, 1523 (2011).
- [30] N. Goldman, G. Juzeliūnas, P. Öhberg, and I. B. Spielman, Light-induced gauge fields for ultracold atoms, *Rep. Prog. Phys.* **77**, 126401 (2014).
- [31] V. Galitski and I. B. Spielman, Spin-orbit coupling in quantum gases, *Nature (London)* **494**, 49 (2013).
- [32] H. Zhai, Degenerate quantum gases with spin-orbit coupling: a review, *Rep. Prog. Phys.* **78**, 026001 (2015).
- [33] N. R. Cooper, J. Dalibard, and I. B. Spielman, Topological Bands for Ultracold Atoms, arXiv:1803.00249.
- [34] D.-W. Zhang, Y.-Q. Zhu, Y. X. Zhao, H. Yan, and S.-L. Zhu, Topological quantum matter with cold atoms, arXiv:1810.09228.
- [35] S.-L. Zhu, B. Wang, and L.-M. Duan, Simulation and Detection of Dirac Fermions with Cold Atoms in an Optical Lattice, *Phys. Rev. Lett.* **98**, 260402 (2007).
- [36] L.-K. Lim, J.-N. Fuchs, and G. Montambaux, Bloch-Zener oscillations across a merging transition of Dirac points, *Phys. Rev. Lett.* **108**, 175303 (2012).
- [37] L. Tarruell, D. Greif, T. Uehlinger, G. Jotzu, and T. Esslinger, Creating, moving and merging Dirac points with a Fermi gas in a tunable honeycomb lattice, *Nature (London)* **483**, 302 (2012).
- [38] L. Duca, T. Li, M. Reitter, I. Bloch, M. Schleier-Smith, and U. Schneider, An Aharonov-Bohm interferometer for determining Bloch band topology, *Science* **347**, 288 (2015).
- [39] D. R. Hofstadter, Energy levels and wave functions of Bloch electrons in rational and irrational magnetic fields, *Phys. Rev. B* **14**, 2239 (1976); P. G. Harper, The general motion of conduction electrons in a uniform magnetic field, with application to the diamagnetism of metals, *Proc. Phys. Soc. London, Sect. A* **68**, 874 (1955).
- [40] F. D. M. Haldane, Model for a quantum Hall effect without Landau levels: Condensed-matter realization of the “parity anomaly”, *Phys. Rev. Lett.* **61**, 2015 (1988).
- [41] H. Miyake, G. A. Siviloglou, C. J. Kennedy, W. C. Burton, and W. Ketterle, Realizing the Harper Hamiltonian with laser-assisted tunneling in optical lattices, *Phys. Rev. Lett.* **111**, 185302 (2013).
- [42] M. Aidelsburger, M. Atala, M. Lohse, J. T. Barreiro, B. Paredes, and I. Bloch, Realization of the Hofstadter Hamiltonian with ultracold atoms in optical lattices, *Phys. Rev. Lett.* **111**, 185301 (2013).
- [43] M. Aidelsburger, M. Lohse, C. Schweizer, M. Atala, J. T. Barreiro, S. Nascimbène, N. R. Cooper, I. Bloch, and N. Goldman, Measuring the Chern number of Hofstadter bands with ultracold bosonic atoms, *Nat. Phys.* **11**, 162 (2015).
- [44] L. B. Shao, S.-L. Zhu, L. Sheng, D. Y. Xing, and Z. D. Wang, Realizing and detecting the quantum Hall effect without Landau levels by using ultracold atoms, *Phys.*

- Rev. Lett. **101**, 246810 (2008).
- [45] G. Jotzu, M. Messer, R. Desbuquois, M. Lebrat, T. Uehlinger, D. Greif, and T. Esslinger, Experimental realisation of the topological Haldane model with ultracold fermions, *Nature (London)* **515**, 237 (2014).
 - [46] M. Mancini, G. Pagano, G. Cappellini, L. Livi, M. Rider, J. Catani, C. Sias, P. Zoller, M. Inguscio, M. Dalmonte, and L. Fallani, Observation of chiral edge states with neutral fermions in synthetic Hall ribbons, *Science* **349**, 1510 (2015).
 - [47] B. K. Stuhl, H.-I. Lu, L. M. Aycock, D. Genkina, and I. B. Spielman, Visualizing edge states with an atomic Bose gas in the quantum Hall regime, *Science* **349**, 1514 (2015).
 - [48] D. J. Thouless, Quantization of particle transport, *Phys. Rev. B* **27**, 6083 (1983); Q. Niu, Towards a quantum pump of electric charges, *Phys. Rev. Lett.* **64**, 1812 (1990).
 - [49] L. Wang, M. Troyer, and X. Dai, Topological Charge Pumping in a One-Dimensional Optical Lattice, *Phys. Rev. Lett.* **111**, 026802 (2013); D.-W. Zhang, F. Mei, Z.-Y. Xue, S.-L. Zhu, and Z. D. Wang, Simulation and measurement of the fractional particle number in one-dimensional optical lattices, *Phys. Rev. A* **92**, 013612 (2015); F. Mei, J.-B. You, D.-W. Zhang, X.-C. Yang, R. Fazio, S.-L. Zhu, and L. C. Kwek, Topological insulator and particle pumping in a one-dimensional shaken optical lattice, *Phys. Rev. A* **90**, 063638 (2014); X.-F. Zhou, J.-S. Pan, Z.-X. Liu, W. Zhang, W. Yi, G. Chen, and S.-T. Jia, Symmetry-protected topological states for interacting fermions in Alkaline-Earth-like atoms, *Phys. Rev. Lett.* **119**, 185701 (2017).
 - [50] S. Nakajima, T. Tomita, S. Taie, T. Ichinose, H. Ozawa, L. Wang, M. Troyer, and Y. Takahashi, Topological Thouless pumping of ultracold fermions, *Nat. Phys.* **12**, 296 (2016).
 - [51] M. Lohse, C. Schweizer, O. Zilberberg, M. Aidelsburger, and I. Bloch, A Thouless quantum pump with ultracold bosonic atoms in an optical superlattice, *Nat. Phys.* **12**, 350 (2016).
 - [52] H.-I. Lu, M. Schemmer, L. M. Aycock, D. Genkina, S. Sugawa, and I. B. Spielman, Geometrical Pumping with a Bose-Einstein Condensate, *Phys. Rev. Lett.* **116**, 200402 (2016).
 - [53] M. Lohse, C. Schweizer, H. M. Price, O. Zilberberg, and I. Bloch, Exploring 4D quantum Hall physics with a 2D topological charge pump, *Nat. Phys.* **10**, 1038 (2018).
 - [54] X.-J. Liu, K. T. Law, and T. K. Ng, Realization of 2D spin-orbit interaction and exotic topological orders in cold atoms, *Phys. Rev. Lett.* **112**, 086401 (2014).
 - [55] Z. Wu, L. Zhang, W. Sun, X.-T. Xu, B.-Z. Wang, J.-C. Ji, Y. Deng, S. Chen, X.-J. Liu, J.-W. Pan, Realization of two-dimensional spin-orbit coupling for Bose-Einstein condensates, *Science* **354**, 83 (2016).
 - [56] J. H. Jiang, Tunable topological Weyl semimetal from simple-cubic lattices with staggered fluxes, *Phys. Rev. A* **85**, 033640 (2012).
 - [57] Y. Xu, R.-L. Chu, and C. Zhang, Anisotropic Weyl Fermions from the Quasiparticle Excitation Spectrum of a 3D Fulde-Ferrell Superfluid, *Phys. Rev. Lett.* **112**, 136402 (2014); Y. Xu, F. Zhang, and C. Zhang, Structured Weyl Points in Spin-Orbit Coupled Fermionic Superfluids, *Phys. Rev. Lett.* **115**, 265304 (2015).
 - [58] B. Liu, X. Li, L. Yin, and W. V. Liu, Weyl Superfluidity in a Three-Dimensional Dipolar Fermi Gas, *Phys. Rev. Lett.* **114**, 045302 (2015).
 - [59] T. Dubcek, C. J. Kennedy, L. Lu, W. Ketterle, M. Soljacic and H. Buljan, Weyl points in three-dimensional optical lattices: synthetic magnetic monopoles in momentum space, *Phys. Rev. Lett.* **114**, 225301 (2015).
 - [60] D.-W. Zhang, S.-L. Zhu, and Z. D. Wang, Simulating and exploring Weyl semimetal physics with cold atoms in a two-dimensional optical lattice, *Phys. Rev. A* **92**, 013632 (2015).
 - [61] S. Ganeshan and S. Das Sarma, Constructing a Weyl semimetal by stacking one-dimensional topological phases, *Phys. Rev. B* **91**, 125438 (2015).
 - [62] W.-Y. He, S. Zhang, and K. T. Law, Realization and detection of Weyl semimetals and the chiral anomaly in cold atomic systems, *Phys. Rev. A* **94**, 013606 (2016).
 - [63] Z. Li, H.-Q. Wang, D.-W. Zhang, S.-L. Zhu, and D.-Y. Xing, Dynamics of Weyl quasiparticles in an optical lattice, *Phys. Rev. A* **94**, 043617 (2016).
 - [64] Y. Xu and L.-M. Duan, Type-II Weyl points in three-dimensional cold-atom optical lattices, *Phys. Rev. A* **94**, 053619 (2016).
 - [65] X. Kong, J. He, Y. Liang, and S.-P. Kou, Tunable Weyl semimetal and its possible realization in optical lattices, *Phys. Rev. A* **95**, 033629 (2017).
 - [66] K. Shastri, Z. Yang, and B. Zhang, Realising type II Weyl points in an optical lattice, *Phys. Rev. B* **95**, 014306 (2017).
 - [67] X. Y. Mai, D.-W. Zhang, Z. Li, and S.-L. Zhu, Exploring topological double-Weyl semimetals with cold atoms in optical lattices, *Phys. Rev. A* **94**, 053633 (2017).
 - [68] L. Lepori, I. C. Fulga, A. Trombettoni, and M. Burrello, Double Weyl points and Fermi arcs of topological semimetals in non-Abelian gauge potentials, *Phys. Rev. A* **94**, 053633 (2016).
 - [69] X. Tan, D.-W. Zhang, Q. Liu, G. Xue, H.-F. Yu, Y.-Q. Zhu, H. Yan, S.-L. Zhu, and Y. Yu, Topological Maxwell Metal Bands in a Superconducting Qutrit, *Phys. Rev. Lett.* **120**, 130503 (2018).
 - [70] H. Hu and C. Zhang, Spin-1 topological monopoles in parameter space of ultracold atoms, *Phys. Rev. A* **98**, 013627 (2018).
 - [71] S.-T. Wang, D.-L. Deng, and L.-M. Duan, Probe of Three-Dimensional Chiral Topological Insulators in an Optical Lattice, *Phys. Rev. Lett.* **113**, 033002 (2014).
 - [72] E. Alba, X. Fernandez-Gonzalvo, J. Mur-Petit, J. K. Pachos, and J. J. Garcia-Ripoll, Seeing Topological Order in Time-of-Flight Measurements, *Phys. Rev. Lett.* **107**, 235301 (2011).
 - [73] P. Hauke, M. Lewenstein, and A. Eckardt, Tomography of Band Insulators from Quench Dynamics, *Phys. Rev. Lett.* **113**, 045303 (2014).
 - [74] D.-L. Deng, S.-T. Wang, and L.-M. Duan, Direct probe of topological order for cold atoms, *Phys. Rev. A* **90**, 041601(R) (2014).
 - [75] D.-W. Zhang, Y. X. Zhao, R.-B. Liu, Z.-Y. Xue, S.-L. Zhu, and Z. D. Wang, Quantum simulation of exotic PT-invariant topological nodal loop bands with ultracold atoms in an optical lattice, *Phys. Rev. A* **93**, 043617 (2016).
 - [76] N. Flaschner, B. S. Rem, M. Tarnowski, D. Vogel, D.-S. Luhmann, K. Sengstock, and C. Weitenberg, Experimental reconstruction of the Berry curvature in a Floquet Bloch band, *Science* **352**, 1091 (2016).

- [77] T. Li, L. Duca, M. Reitter, F. Grusdt, E. Demler, M. Endres, M. Schleier-Smith, I. Bloch, and U. Schneider, Bloch state tomography using Wilson lines, *Science* **352**, 1094 (2016).
- [78] L. Wang, A. A. Soluyanov, and M. Troyer, Proposal for direct measurement of topological invariants in optical lattices, *Phys. Rev. Lett.* **110**, 166802 (2013).
- [79] R. D. King-Smith and D. Vanderbilt, Theory of polarization of crystalline solids, *Phys. Rev. B* **47**, 1651 (1993); S. Coh and D. Vanderbilt, Electric Polarization in a Chern Insulator, *Phys. Rev. Lett.* **102**, 107603 (2009).
- [80] N. Marzari, A. Mostofi, J. R. Yates, I. Souza, and D. Vanderbilt, Maximally localized Wannier functions: Theory and applications, *Rev. Mod. Phys.* **84**, 1419 (2012).